Electrochimica Acta 137 (2014) 83–90

Contents lists available at ScienceDirect

Electrochimica Acta

journal homepage: www.elsevier.com/locate/electacta

An Electrochemical Study of H_2O_2 Oxidation and Decomposition on Simulated Nuclear Fuel (SIMFUEL)

Linda Wu, David W. Shoesmith*,[1]

Department of Chemistry and Surface Science Western, The University of Western Ontario, London, ON, N6A 5B7, Canada

ARTICLE INFO

Article history:
Received 14 February 2014
Received in revised form 2 June 2014
Accepted 2 June 2014
Available online 6 June 2014

Keywords:
Used nuclear fuel
UO_2 corrosion
H_2O_2 decomposition

ABSTRACT

The anodic oxidation and open circuit decomposition of H_2O_2 on UO_{2+x} surfaces have been investigated voltammetrically and using linear polarization resistance measurements over the pH range 9.5 to 12.6. At the lower pH values both the anodic oxidation and decomposition reactions are almost completely blocked by a thin surface layer of U^{VI} oxide. At higher pH this layer becomes more soluble and anodic oxidation occurs on the sublayer of $U^{IV}_{1-2x}U^{V}_{2x}O_{2+x}$, but is partially controlled by transport through a permeable, chemically dissolving U^{VI} oxide/hydroxide layer. At positive electrode potentials (0.3 V vs. saturated calomel electrode), approximately 70% of the anodic current is consumed by H_2O_2 oxidation the remaining 30% going to produce $U^{VI}O_2(OH)_x^{(2-x)+}$. At higher pH values, H_2O_2 decomposition occurs on an unblocked $U^{IV}_{1-2x}U^{V}_{2x}O_{2+x}$ surface and the pH dependence of the reaction suggests HO_2^- is the electroactive form of peroxide

1. Introduction

The recommended approach for the long-term management of spent nuclear fuel in Canada is Adaptive Phased Management that includes centralized containment and the isolation of the spent fuel in a deep geological repository. This approach is based on a sequence of barriers, which includes fuel bundles, durable metal containers with an outer barrier of copper and an inner carbon steel vessel, a clay buffer, and a deep stable geological environment [1]. The prospects for long term containment are very promising, and corrosion models predict only minimal corrosion damage insufficient to cause failure [2,3]. However, it is judicious to assess the consequences of container failure leading to exposure of the fuel to groundwater. When the waste container fails, groundwater will flood the container and contact the spent fuel leading to the release of radionuclides.

The uranium dioxide fuel is very insoluble with a low dissolution rate under reducing conditions, but the solubility increases by orders of magnitude under oxidizing conditions making the fuel susceptible to corrosion [4]. The concentration of dissolved oxidants in the groundwater contacting the fuel is expected to be very low, since environmental oxidants (specifically dissolved O_2) will have been consumed by container corrosion and mineral/biological oxidation processes prior to container failure. However, the radiation fields associated with the fuel will produce oxidants (e.g., $OH^\bullet$, H_2O_2, O_2) by water radiolysis and these radiolytic oxidants will sustain oxidizing conditions leading to corrosion of the fuel and an increase of radionuclide release rates.

Provided that the waste container isolates the fuel from groundwater for a few hundred years, only alpha radiation fields will remain capable of producing significant oxidant concentrations. For alpha radiolysis, H_2O_2 has been demonstrated to be the key oxidant for fuel corrosion [5–7] and extensive study of H_2O_2 reduction on UO_2 has been undertaken [8–12]. Goldik et al. studied the electrochemical kinetics and mechanism for H_2O_2 reduction on SIMFUEL pellets [8,11,13,14], UO_2 specimens doped with simulated fission products to mimic the effect of in-reactor irradiation [15]. They showed that the cathodic reduction of H_2O_2 is catalyzed by the ability of H_2O_2 to create its own U^{IV}/U^{V} donor-acceptor sites

$$2U^{IV} + H_2O_2 \rightarrow 2U^{V} + 2OH^- \quad (1)$$

followed by the electrochemical regeneration of the U^{IV} sites,

$$2U^{V} + 2e^- \rightarrow 2U^{IV} \quad (2)$$

The H_2O_2 reduction rate is independent of pH between pH 4 and 9, but suppressed at more alkaline values. The reduction of H_2O_2 is only weakly dependent on applied potential with a fractional reaction order with respect to H_2O_2, consistent with partial control by the chemical reaction (1) [11]. At low overpotentials, H_2O_2

* Corresponding author. Tel.: +1 519 661 2111x86366; fax: +1 519 661 3022.
E-mail address: dwshoesm@uwo.ca (D.W. Shoesmith).
[1] ISE member.

http://dx.doi.org/10.1016/j.electacta.2014.06.002
0013-4686/

reduction proceeds significantly faster on the noble metal particles within the SIMFUEL than on the UO_{2+x} lattice surface [13].

Under corrosion conditions there are two competitive anodic reactions which can couple with the cathodic reduction of H_2O_2: the oxidative dissolution of UO_2 and the simultaneous oxidation of H_2O_2, the latter leading to H_2O_2 decomposition.

$$2H_2O_2 \rightarrow O_2 + 2H_2O \quad (3)$$

The rates of fuel corrosion and H_2O_2 decomposition are determined by the fraction of each anodic reaction. Early studies on H_2O_2 decomposition have been reviewed [5,16]. In a UO_2 dissolution experiment in H_2O_2-containing solution, de Pablo et al. [17] measured both U release to solution and the H_2O_2 consumption rate. Since more H_2O_2 was consumed than U released it was calculated that H_2O_2 decomposition was also occurring although an inability to account for oxidized U retained on the surface as a corrosion product deposit made the measurement only qualitative. An accumulation of gas bubbles on UO_2 surfaces in the presence of H_2O_2 has been observed suggesting that a UO_2 surface can catalyze H_2O_2 decomposition [16,18]. Christensen et al. [19] also claimed that H_2O_2 decomposition was occurring in borax buffer solutions ($pH = 8 \pm 0.2$) based on a discrepancy between the amount of dissolved U analyzed compared to the amount expected if all the H_2O_2 consumed had caused dissolution. Recent leaching experiments [7,20,21] confirmed that only a portion of consumed H_2O_2 was involved in UO_2 corrosion, although the exact fraction varied with different UO_2 specimens (e.g., unirradiated UO_2, doped UO_2 and SIMFUEL).

Sunder et al. [16] found the corrosion potential of UO_2 (as opposed to SIMFUEL) in H_2O_2-containing solutions to be independent of $[H_2O_2]$ over the range 10^{-5} to 10^{-2} mol.L^{-1} and attributed this to the blockage of both decomposition and UO_2 dissolution by the presence of a U^{VI} layer on the electrode surface. A more comprehensive study in the presence of the α-radiolysis of water [22], to produce the oxidant H_2O_2, appeared to confirm this claim. The coupled reactions of H_2O_2 reduction and oxidation appeared to be buffered at pH = 9.5 and the slow rate of H_2O_2 decomposition was attributed to surface coverage by insulating U^{VI} species only slowly released by chemical dissolution as UO_2^{2+} in non-complexing solution. Since this U^{VI} species blocked the underlying conducting substrate surface the rate of H_2O_2 decomposition was limited by the rate of its release to solution. If this mechanism is correct, then decomposition is inhibited by the extent of surface oxidation under open-circuit (corrosion) conditions.

In addition, the rate of H_2O_2 decomposition depends on the alkalinity of the solution. Haines and McCracken [23] reported that the decomposition rate in a LiOH solution (pH 10.3) was 4-5 times that in neutral pH water. Navarro et al. [24] observed that H_2O_2 decomposed rapidly in aerated NaOH solutions with the maximum rate being attained in the pH range 11.5 to 11.7. Since this pH coincided with the first pK_a value of H_2O_2, it was proposed that the presence of both H_2O_2 and the hydroperoxide anion (HO_2^-) was necessary for uncatalyzed decomposition according to previously suggested mechanisms [25,26]. Electrochemical studies [27,28] showed that H_2O_2 oxidation could proceed at lower potentials in more alkaline solutions. While this was attributed to the involvement of protons in the H_2O_2 oxidation reaction the details of the mechanism were not elucidated.

Here, we present a more extensive study of H_2O_2 oxidation and decomposition on UO_2 by varying the solution pH, investigating the influence of oxidized surface states (U^V/U^{VI}) on the electrochemical oxidation of H_2O_2, and determining the relative decomposition rates as a function of pH using linear polarization resistance measurements.

2. Experimental

The working electrode was a 12-mm (in diameter) disc cut from simulated spent fuel pellets (SIMFUEL) which were fabricated by Atomic Energy of Canada Limited (Chalk River, Ontario). SIMFUEL is an analogue of CANDU (CANadian Deuterium Uranium) spent nuclear fuel made of natural UO_2 doped with non-radioactive elements to replicate the chemical effects of the fission products produced by in-reactor burn-up [29]. This material provides a practical means to study the chemical properties (corrosion behaviour in this study) of spent fuel without the associated radiation fields. The eleven dopants (Sr, Y, Ce, Nd, La, Zr, Ba, Pd, Ru, Mo, Rh) can be divided into two groups: (i) the rare earth elements (RE^{III}) which substitute for U^{IV} in the UO_2 lattice, thereby creating adjacent U^V atoms and increasing donor-acceptor sites for surface redox reactions [30]; (ii) the noble metal dopants (Pd, Ru, Mo, Rh) which congregate as metallic particles in the UO_2 matrix. The SIMFUEL used in this study mimics an in-reactor burn-up of 1.5 atomic %. The working electrode was set in resin so that only the flat front face was exposed to solution. The procedure for electrode preparation has been described previously [11].

All electrochemical measurements were performed in a conventional three-electrode cell. Potentials were measured against a saturated calomel reference electrode (SCE, Fisher Scientific) and all potentials quoted in this study refer to the SCE. The counter electrode was a Pt sheet with a surface area of 6 cm^2 (99.9% pure, Sigma-Aldrich) spot-welded to a Pt wire. The cell was placed in a grounded Faraday cage to minimize external noise. An analytical rotator (Pine Instruments, model ASR) was employed to control the rotation rate of the working electrode. A Solartron model 1287 potentiostat was used to apply potentials and record current responses. Corrware software (Scribner Associates) was used to control the potentiostat and analyze the data.

The working electrode was cathodically cleaned at an applied potential of −1.2 V for 1 min prior to each experiment to remove any air-formed oxides. Cyclic voltammetric and potentiodynamic experiments were conducted at a scan rate of 10 mV.s^{-1}. The positive potential limit of the scan was 0.4 V and the negative limit was varied depending on the purpose of the experiment. In a dissolution experiment, the working electrode was kept at 0.3 V for 4 hours in a small electrochemical cell with a volume of 50 mL. Subsequently, the solution concentration of U was analyzed by inductively coupled plasma atomic emission spectroscopy (ICP-AES).

All experiments were Ar-purged (Ultra high purity, Praxair) and conducted at room temperature. Solutions were prepared using distilled deionized water with a resistance of 18.2 MΩ.cm purified by Millipore milli-Q-plus units. The electrolyte was 0.1 mol.L^{-1} NaCl, and the solution pH was adjusted to a value between 9.5 and 12.6 with NaOH (Caledon Chemical). Hydrogen peroxide (3% w/v, LabChem) was added immediately prior to experiments to obtain a concentration between 0 and 0.02 mol.L^{-1}. An Orion model 250A+ pH meter and Orion 91-07 Triode pH/ATC probe were used to monitor the pH before and after electrochemical measurements.

3. Results and discussion

3.1. Open-circuit potential in H_2O_2 solution

Within the pH range 9.5 to 12.5, the open circuit potential (E_{OC}) was independent of $[H_2O_2]$ over the range 0.004 to 0.02 mol.L^{-1}, Fig. 1, consistent with previous observations at pH = 9.5 [16]. Also shown in the figure are the calculated equilibrium potentials for the redox reactions:

$$H_2O_2 + 2e^- \rightleftarrows 2OH^- \quad (4)$$

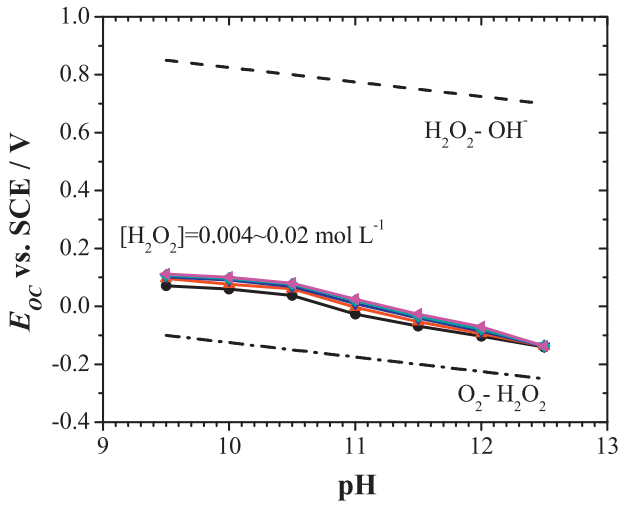

Fig. 1. Open-Circuit Potential (E_{OC}) as a function of pH recorded on a SIMFUEL electrode in solutions containing various [H_2O_2] (0.004~0.02 mol.L^{-1}). The dashed lines indicate the equilibrium potentials for the H_2O_2 reduction and oxidation half reactions calculated assuming a partial pressure for O_2 of 1 atmosphere.

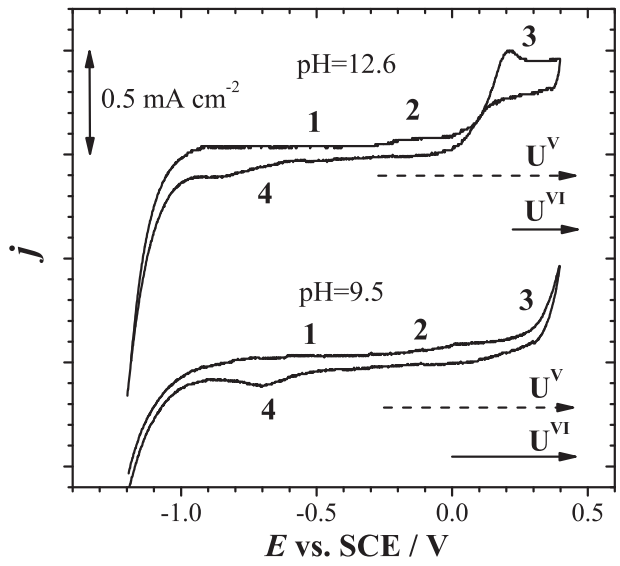

Fig. 2. Voltammograms recorded on a SIMFUEL electrode at pH 9.5 and 12.6; [NaCl] = 0.1 mol.L^{-1}; rotation rate = 16.7 Hz; scan rate = 10 mV.s^{-1}.

and

$$O_2 + 2H^+ + 2e^- \rightleftarrows H_2O_2 \quad (5)$$

which can couple to yield the overall decomposition, reaction (3).

As discussed previously [16,22], this independence of E_{OC} on [H_2O_2] could be interpreted in one of two ways: (i) as the [H_2O_2] is increased, the kinetics of both the anodic and cathodic reactions are equally affected, leading to a condition of redox buffering (i.e., an increase in decomposition rate without a change in E_{OC}); (ii) the overall decomposition reaction is independent of [H_2O_2], as would be the case if the rate were controlled by the rate of release of the U^{VI} species from the surface to the solution.

Inspection of Fig. 1 shows two additional notable features: E_{OC} was closer to the equilibrium potential for the anodic half reaction (5) than the cathodic half reaction (4); and the dependence of E_{OC} on [H_2O_2] changes between pH = 10.5 and 11.0. The proximity of E_{OC} to $(E_e)_{anod}$ implied that, for the decomposition reaction, the anodic reaction was rapid and, hence, the potential-determining reaction, while the overall reaction was controlled by the kinetics of the cathodic half reaction. However, this presumption does not take into account that the decomposition reaction is effectively blocked by a U^{VI} surface layer. The change in slope between pH = 10.5 and 11.0 would then indicate a change in surface state leading to an acceleration of the H_2O_2 oxidation reaction.

3.2. Effect of pH on voltammetry

Fig. 2 shows cyclic voltammograms recorded at pH 9.5 and 12.5 in H_2O_2-free solutions. The various stages of oxidation and reduction generally seen [5,12] are numbered on the plot. Stage 1, which is associated with the anodic oxidation of non-stoichiometric surface locations, appeared to be insignificant on the stoichiometric SIMFUEL used in these experiments. The shallow shoulder in region 2 has been shown to be due to the anodic oxidation of the stoichiometric surface

$$UO_2 + xH_2O \rightarrow U^{IV}_{1-2x}U^{V}_{2x}O_{2+x} + 2xH^+ + 2xe^- \quad (6)$$

and was slightly more prominent at pH = 12.5 compared to 9.5, indicating a thicker and/or more intensively oxidized layer was formed. The most significant difference in anodic oxidation behaviour between the two pHs was in region 3, for potentials ≥ 0.1 V. In neutral solutions, the surface was further oxidized to a passivating U^{VI} layer (commonly designated $UO_3.yH_2O$) and some soluble UO_2^{2+}. Hydrolysis of this dissolved uranyl ion then leads to local acidification

$$UO_2^{2+} + yH_2O \rightarrow (UO_2)(OH)_y^{(2-y)+} + yH^+ \quad (7)$$

and local dissolution of the U^{VI} surface layer

$$UO_3 \cdot yH_2O + 2H^+ \rightarrow UO_2^{2+} + (y+1)\ \ H_2O \quad (8)$$

This would account for the steep rise in current for $E > 0.3$ V, leading to extensive, but localized dissolution of the UO_2 surface.

In alkaline solution, U^{VI} is over two orders of magnitude more soluble than in neutral solution [31] and passivation was avoided, the current rising rapidly as extensive dissolution occurred for $E \geq 0.1$ V,

$$U^{IV}_{1-2x}U^{V}_{2x}O_{2+x} + 3OH^- \rightarrow U^{VI}O_{2+x}(OH)_3^{(1+2x)-} + (2-2x)\ \ e^- \quad (9)$$

For potentials ≥ 0.2 V, the current plateau showed that anodic dissolution was controlled by a nonelectrochemical process, most likely the chemical dissolution of a U^{VI} surface layer as discussed elsewhere [12]. The constant current for potentials in the range 0.2 V to 0.4 V would then indicate that this surface U^{VI} layer increased in thickness with increasing potential. That this surface layer was not passivating was confirmed on the reverse scan, a substantial anodic current being observed until the potential fell below ~ 0.1 V. Additionally, a cathodic peak in region 4 for the reduction of oxidized surface layers was observed. The charge associated with this peak is approximately the same as that for the reduction of the oxidized layer formed at pH = 9.5, confirming that the majority of the charge on the anodic scan at pH = 12.6 went to the production of soluble UO_2^{2+}.

The chemical composition of the UO_2 surface at these two pH values has been determined previously by X-ray photoelectron spectroscopy (XPS) [12,32] and the ranges over which the composition changes are indicated by the arrows in Fig. 2. While the onset of oxidation to produce U^V is similar at both pH values, the surface accumulation of U^{VI} at the higher pH is delayed by more extensive dissolution.

3.3. Effect of pH on H_2O_2 oxidation

Fig. 3 shows the anodic current recorded during anodic scans in solutions containing 0.02 mol.L^{-1} H_2O_2 at both pH values. The

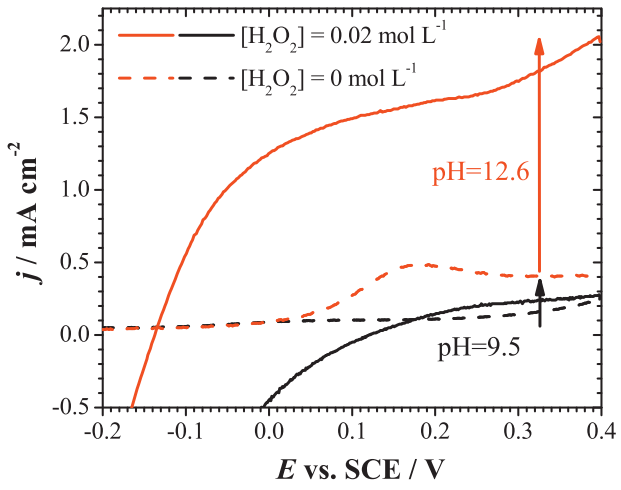

Fig. 3. Anodic current density recorded on a SIMFUEL electrode in a H_2O_2 solution at pH 9.5 and 12.6; [NaCl] = 0.1 mol.L^{-1}; rotation rate = 25 Hz; scan rate = 10 mV.s^{-1}.

background currents recorded on the forward scan in the absence of H_2O_2 are also shown, as dashed lines, for comparison. The oxidation current at pH = 12.6 was considerably larger than that at pH = 9.5.

At pH = 9.5, the anodic current was almost independent of electrode rotation rate consistent with expectations for a surface covered with a slowly dissolving insulating layer of U^{VI}, Fig. 4(a).

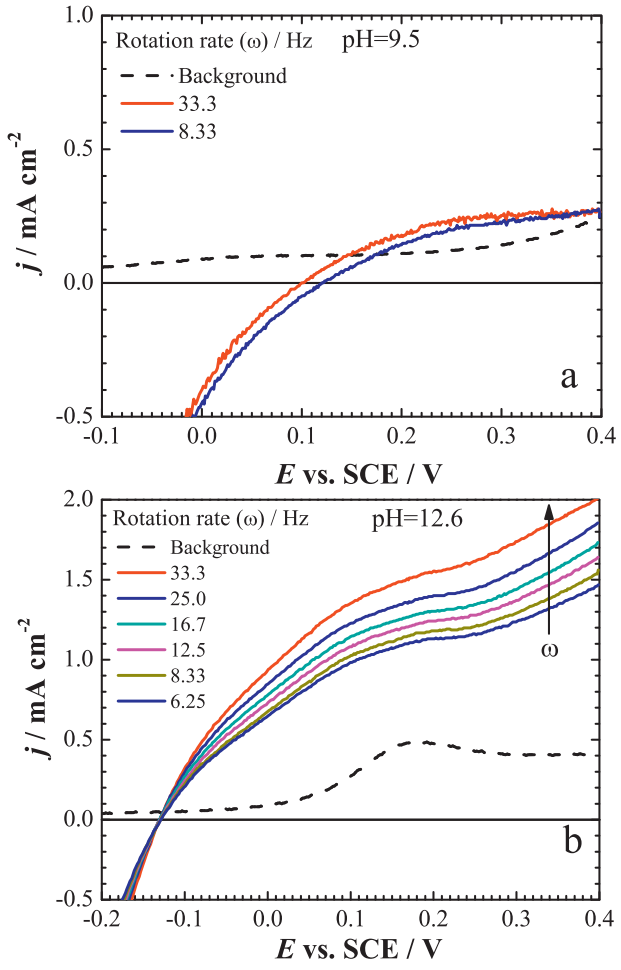

Fig. 4. Anodic current densities recorded on a SIMFUEL electrode at various rotation rates; [NaCl] = 0.1 mol.L^{-1}; [H_2O_2] = 0 (as background) or 0.02 mol.L^{-1}; (a) pH = 9.5 and (b) pH = 12.6.

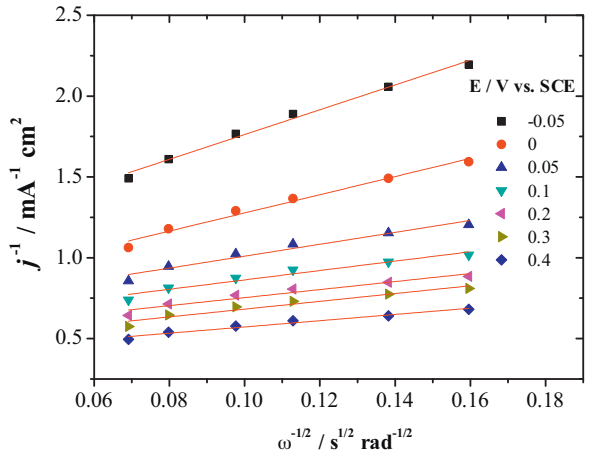

Fig. 5. Koutecky-Levich plot (current density^{-1} versus rotation rate$^{-1/2}$) derived from Fig. 4(b) at different potentials.

At pH = 12.6, the anodic current became dependent on electrode rotation rate, Fig. 4(b). The diffusion-limited current density, j_d, for the anodic oxidation of H_2O_2 to O_2 can be calculated using the expression

$$j_d = B\omega^{1/2} \tag{10}$$

$$B = 0.62nF\gamma^{-1/6}D_{H_2O_2}^{2/3}C_{H_2O_2} \tag{11}$$

where ω is the angular velocity of rotation, n the number of electrons exchanged per molecule of H_2O_2, F the Faraday constant, γ the kinematic viscosity of the electrolyte, D_{H2O2} the H_2O_2 diffusion coefficient and C_{H2O2} the bulk H_2O_2 concentration in the electrolyte. Using appropriate values ($n = 2$, $\gamma = 10^{-2}$ cm^2.s^{-1}, $D_{H2O2} = 10^{-5}$ cm^2.s^{-1}, $C_{H2O2} = 2 \times 10^{-5}$ mol.cm^{-3}), the j_d was determined to be 15.0–34.6 mA.cm^{-2} for the ω range used in Fig. 4(b).

The currents in Fig. 4(b) are plotted according to the first-order Koutecky-Levich equation [33]

$$\frac{1}{j} = \frac{1}{j_k} + \frac{1}{B\omega^{1/2}} \tag{12}$$

in Fig. 5, where j is the measured current density and j_k is the kinetic current density (in absence of any mass transfer effect). The parallel straight lines are consistent with the reaction being first order with respect to H_2O_2. The kinetic currents (j_k) obtained by extrapolation of these plots to infinite rotation rate are in the range 1.0 to 2.6 mA.cm^{-2} over the potential range, −0.05 to 0.4 V. These values are less than 10% of the diffusion-limited current density (15.0–34.6 mA.cm^{-2}), and are plotted in the Tafel form in Fig. 6. The slope of the line (1430 mV/dec) is much higher than that expected for an unimpeded two-electron process (60 mV/dec). Since two anodic processes are possible in this potential range an unequivocal interpretation of this plot cannot be made, but it is reasonable to conclude that the almost potential independent current suggests control of H_2O_2 oxidation by the presence of a permeable insulating U^{VI} oxide/hydroxide surface layer. The most likely controlling reaction step is the transport of H_2O_2 through this surface layer followed by its anodic oxidation on the underlying conductive U^{IV}/U^{V} surface layer. The slight increase in current as the potential increases, Fig. 6, suggests a change in properties of the surface film (decreased thickness; increased dissolution rate) as the potential is made more positive.

That the current was suppressed by the anodic formation of an oxidized surface layer was confirmed by a series of dual scan experiments, in which the potential was scanned from various negative values to +0.4 V and then back to the original negative potential limit followed by a second scan between the same two potentials.

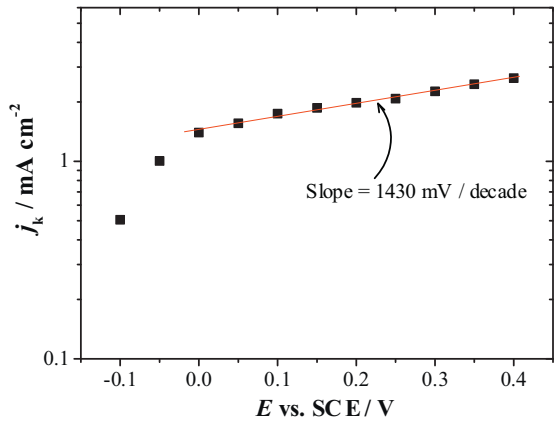

Fig. 6. Plot of the kinetic current density (obtained from the Koutecky-Levich analysis) as a function of potential.

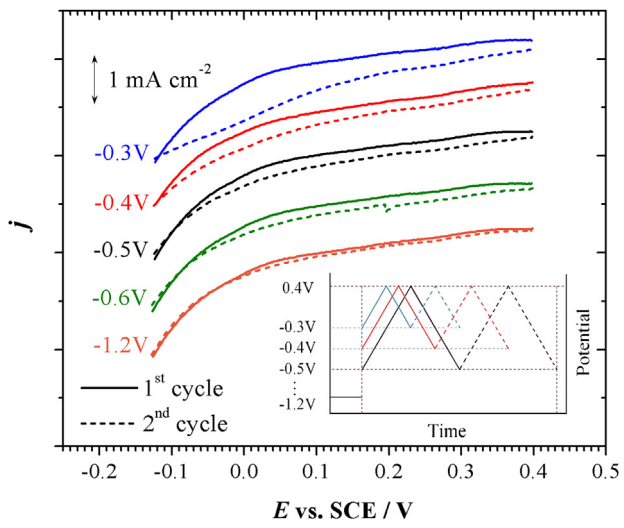

Fig. 7. Anodic current density recorded for various potential scan ranges. Each color indicates a scan from a different cathodic potential vertex as shown in the inset. Solid lines, 1st forward scan; dashed lines, 2nd forward scan; [NaCl] = 0.1 mol.L^{-1}; [H_2O_2] = 0.02 mol.L^{-1}; pH = 12.5.

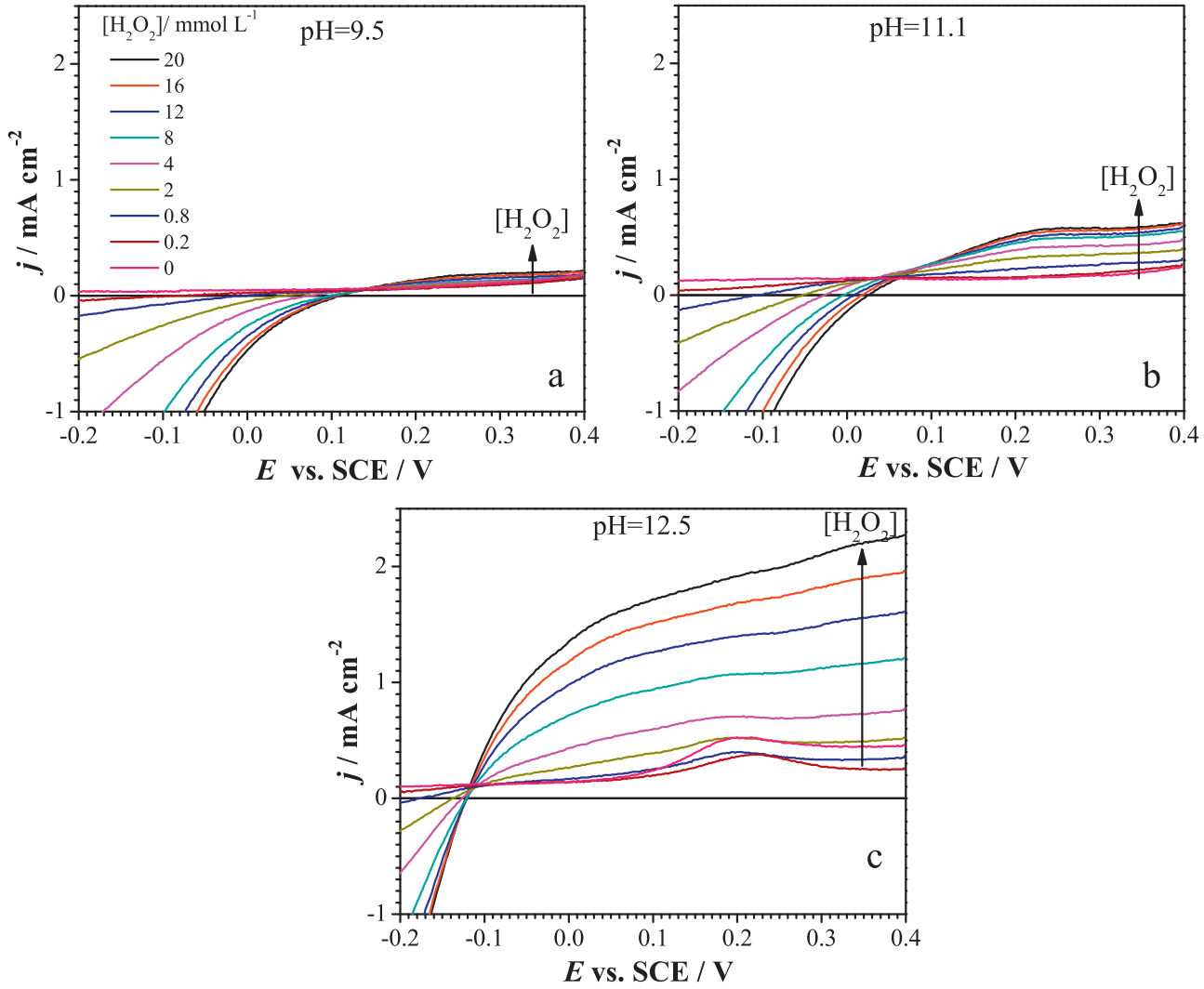

Fig. 8. Anodic current densities recorded in solutions containing various [H_2O_2] (the arrows indicate an increase from 0 to 0.02 mol.L^{-1}) at various pH (a) 9.5, (b) 11.1 and (c) 12.5; rotation rate = 25 Hz; scan rate = 15 mV.s^{-1}.

This procedure was repeated for a sequence of increasingly negative initial potentials, as indicated in the inset to Fig. 7, although the currents recorded at potentials <−0.125 V are not shown for clarity. This figure shows that the anodic current on the second scan was suppressed until the negative limit of the potential was made sufficiently negative (<−0.6 V) to cathodically remove the film formed on the first scan. This observation is consistent with the cv in Fig. 2 which showed that the oxidized layer formed anodically in alkaline solutions was not cathodically reduced until the potential was in the range −0.7 V to −0.9 V.

A series of cv scans was recorded at various $[H_2O_2]$ and pH values, Fig. 8. At all pH values the cathodic reduction of H_2O_2 proceeded rapidly, the current increasing exponentially with a strong dependence on $[H_2O_2]$, over the potential range 0 to −0.2 V; i.e., within region 2 in Fig. 2. In this potential region the surface composition would be $U^{IV}_{1-2x}U^{V}_{2x}O_{2+x}$ with the U^{V} content decreasing as the potential became more negative. A detailed study of H_2O_2 reduction has been published elsewhere [11].

The oxidation currents were strongly dependent on the pH value. At pH = 9.5, the current increase when H_2O_2 was added was marginal. However, in more alkaline solutions the oxidation currents were considerably larger than the background current ($[H_2O_2] = 0$) confirming H_2O_2 oxidation was becoming more significant. At pH = 11.1 the anodic current plateau in the potential range 0.2 V to 0.4 V reflected the suppression of the H_2O_2 oxidation reaction by the U^{VI} surface layer. As the pH was increased further (e.g., to 12.5) the current became more dependent on $[H_2O_2]$. The possibility of a contribution to the current at very positive potentials from H_2O_2 oxidation on the noble metal particles present in SIMFUEL electrodes is under investigation.

Fig. 9 shows the anodic currents recorded at 0.15 V and 0.3 V, taken from the profiles in Fig. 8, for various pH values (9.5 to 12.5) as a function of $[H_2O_2]$. Identical behaviour was observed over the potential range 0.1 V to 0.3 V. At the lower end of the pH scale the current was independent of $[H_2O_2]$ except for a marginal dependence at the lowest concentrations. As the pH was increased above 10.5 the current increased markedly and became increasingly dependent on $[H_2O_2]$. At pH ≥ 11.6 the current approached a first order dependence on $[H_2O_2]$ providing the concentration was not too high. A first order dependence on $[H_2O_2]$ under kinetically controlled oxidation (Fig. 6) on a surface covered by a partially insulating U^{VI} oxide/hydroxide layer is consistent with the anodic oxidation of H_2O_2 occurring by transport through a permeable U^{VI} surface layer.

The overall increase in current with pH can be attributed to one, or both, of two features. Fig. 10 shows the anodic current at 0.3 V ($[H_2O_2] = 0.02$ mol.L^{-1}) plotted as a function of pH and compared to the concentrations of H_2O_2 and HO_2^- calculated using the accepted pK_a value of 11.6 [34] for the dissociation reaction

$$H_2O_2 \rightleftarrows HO_2^- + H^+ \quad (13)$$

The similarity between the anodic current and the concentration of HO_2^- indicates the latter was the electroactive form of peroxide as previously observed for Pt [27,35]. Alternatively, since the solubility of U^{VI} increases by > 10^2 over the pH range 9.5 to 12.5 [31], it is possible that the U^{VI} surface layer became thinner and the H_2O_2 oxidation less inhibited as the pH increased. Experiments to separate the importance of these two possibilities are underway.

3.4. Dissolution experiments

Since the anodic current is comprised of two contributions (the dissolution of UO_2 and the oxidation of H_2O_2), an attempt to separate them was made by analyzing the U^{VI} content of the solution after anodic oxidation at 0.3 V for 4 h. The analyzed amount of dissolved UO_2^{2+} was converted to the charge required for oxidative dissolution of UO_2 as UO_2^{2+}. The total anodic charge was obtained by integration of the measured anodic current. The difference between these two charges can be attributed to H_2O_2 oxidation. Over this period of anodic oxidation the charge retained on the

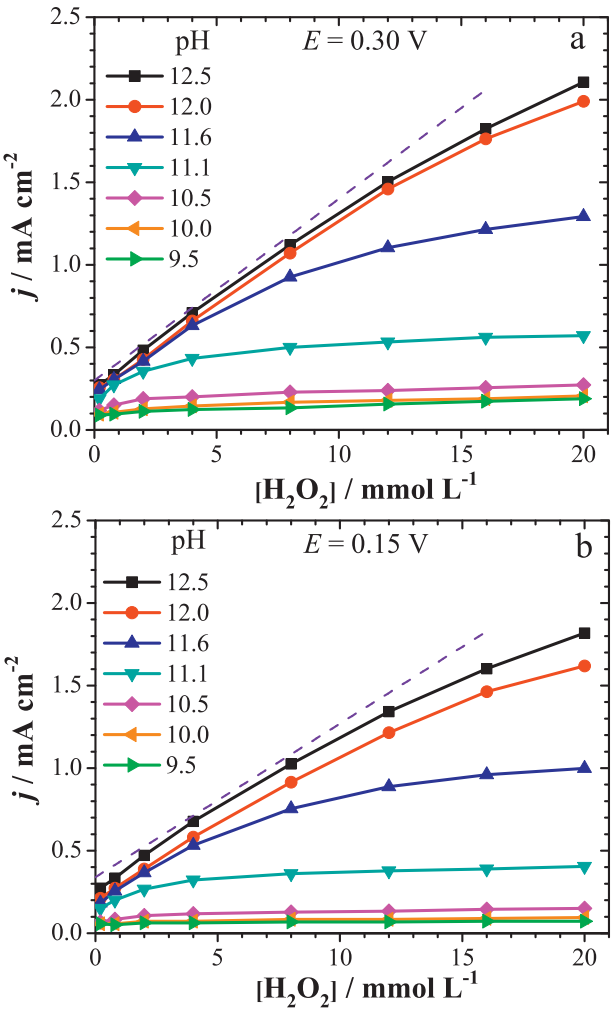

Fig. 9. Anodic current densities recorded at (a) 0.30 V and (b) 0.15 V as a function of $[H_2O_2]$ for various pH values. The dashed line indicates a first order dependence with respect to $[H_2O_2]$.

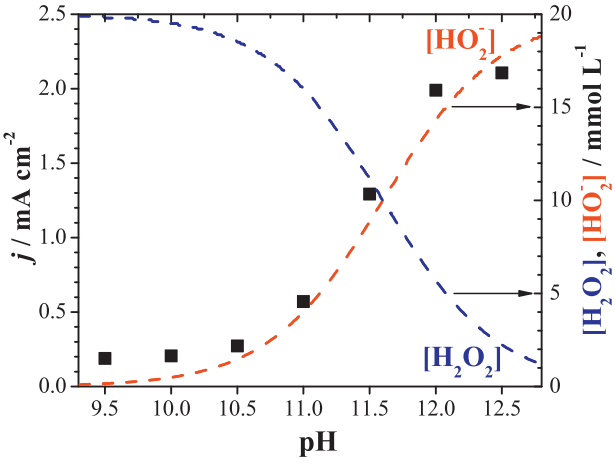

Fig. 10. Current density as a function of pH at 0.3 V in a solution containing $[H_2O_2] = 0.02$ mol.L^{-1}. The dashed curves show the concentrations of the peroxide forms (H_2O_2 and HO_2^-) vs. pH.

Table 1
Distribution of charge between UO_2 oxidative dissolution and H_2O_2 oxidation[a]

	Charge (C)	Fraction of total anodic charge
Total anodic charge	0.0978	100%
Charge due to UO_2 dissolution	0.0279	28.5%
Charge due to H_2O_2 oxidation	0.0699	71.5%

[a] SIMFUEL electrode potentiostaically oxidized at 0.3 V for 4 h in a solution of [NaCl] = 0.1 mol.L^{-1}, [H_2O_2] = 0.02 mol.L^{-1}, pH = 11.0. No rotation was applied.

electrode surface (in the form of oxidized U^{VI} solid) would have been negligible compared to the total charge. As noted in Table 1 the fraction of the current going to H_2O_2 oxidation was 71.5%. Inspection of the cv scans in Fig. 8(b) shows that (for the same conditions as those in the dissolution experiment: pH = 11, E = 0.3 V and [H_2O_2] = 0.02 mol.L^{-1}) the ratio of the anodic currents in H_2O_2-free and H_2O_2-containing solutions is ~ 30%, i.e., about 70% of total current appears to support the oxidation of H_2O_2. The similarity in the charge and current density ratios confirm that the predominant anodic reaction at very positive potentials is H_2O_2 oxidation.

3.5. Polarization resistance measurements

Using the plots in Fig. 4 and Fig. 8 it is possible to measure a polarization resistance (R_P) by measuring the slope of the current–potential plots over the range $E_{OC} \pm 10$ mV. At pH = 9.5, R_P was small since, at a positive E_{OC} of ~ 0.1 V, the surface was blocked by the insulating U^{VI} layer. At pH = 12.6, however, when the surface U^{VI} oxide/hydroxide layer is more soluble and does not block the surface as comprehensively, R_P decreased with electrode rotation rate, Fig. 11, while the value of E_{OC} did not change, Fig. 4(b). This combination of features indicated that the enhanced transport of H_2O_2 to the electrode surface promoted both the anodic and cathodic half reactions coupled at E_{OC}, indicating that the dominant reaction occurring was H_2O_2 decomposition; i.e., the coupling of reactions (4) and (5). When this is the case, the term R_P^{-1} can be considered proportional to the H_2O_2 decomposition rate.

Values of R_P^{-1} measured as a function of [H_2O_2] for a range of pH values are shown in Fig. 12. Since two open circuit reactions are possible, UO_2 corrosion and H_2O_2 decomposition, any measured R_P value is a measure of the resistance to charge transfer of the sum of these two reactions. Presently, the open circuit balance between these reactions is unknown. The analysis in Table 1 shows that ~70% of the current goes to H_2O_2 decomposition under anodic conditions. If a similar balance between

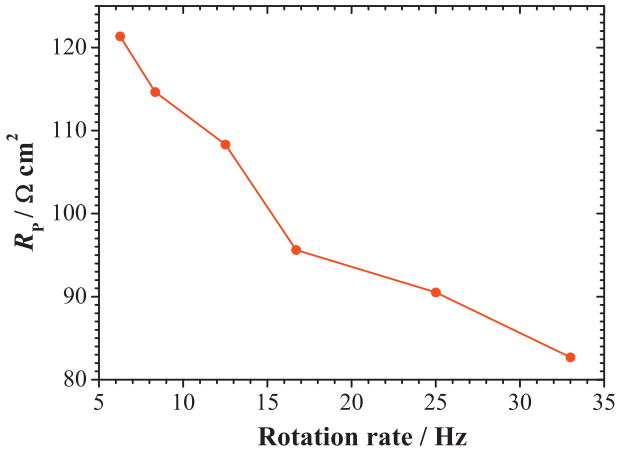

Fig. 11. Polarization resistance, R_p, plotted as a function of rotation rate recorded on a SIMFUEL electrode; [NaCl] = 0.1 mol.L^{-1}; [H_2O_2] = 0.02 mol.L^{-1}; pH = 12.6.

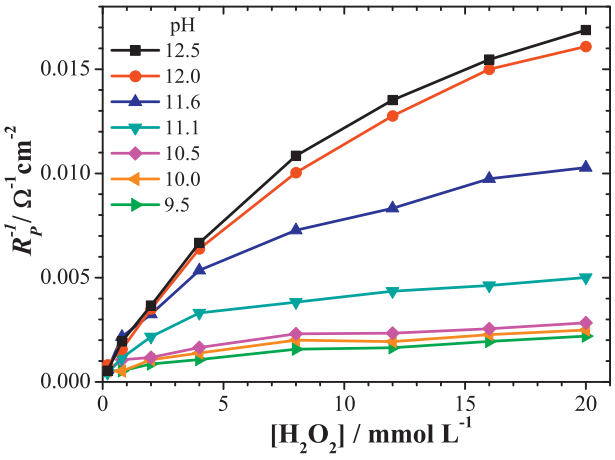

Fig. 12. Reciprocal of the polarization resistance, R_P^{-1}, as a function of [H_2O_2] recorded on a SIMFUEL electrode at various pH values; [NaCl] = 0.1 mol.L^{-1}; rotation rate = 25 Hz.

dissolution and decomposition is assumed to prevail at E_{OC} then the reciprocal of the polarization resistance, R_P^{-1}, can be taken as an approximate measure of the H_2O_2 decomposition rate, at least for high [H_2O_2]. Irrespective of these difficulties it is clear that an increase in pH increases the dependence of the reaction rate on [H_2O_2]. For pH ≤ 10.5, R_P^{-1} was very low and only marginally dependent on [H_2O_2]. As the pH increased to ≥ 11.1 the value of R_P^{-1} increased markedly, and as observed for the anodic currents at applied potentials (Fig. 9) achieved a first order dependence for [H_2O_2] < 5 mmol.L^{-1}. As shown in Fig. 1, E_{OC} varied from ~ 0.1 V at pH = 9.5, when the electrode surface was expected to be covered by a U^{VI} surface layer (Fig. 2), to ~−0.1 V at pH = 12.5 when the surface composition will be relatively free of U^{VI} (Fig. 2) exposing the underlying $U^{IV}_{1-2x}U^{V}_{2x}O_{2+x}$ layer. These results also suggest that the relative importance of the H_2O_2 decomposition reaction increases as [H_2O_2] increases, especially for pH > 11.

The decomposition of H_2O_2 on the surfaces of various metal oxides (usually in particulate form) has been extensively studied [36,37], and a variety of reaction pathways have been discussed. For oxides in which multiple oxidation states do not exist (TiO_2, ZrO_2, SiO_2, Al_2O_3), it has been demonstrated that decomposition occurs on the oxide surface but the details of the mechanism remain unresolved. Recently the reaction on ZrO_2 was shown to involve the formation of OH• as an intermediate species [38]. For decomposition on oxides within which redox transformations are possible (iron oxides being the prime example) decomposition has been shown to involve coupling with redox transformations (e.g. $Fe^{II} \leftrightarrow Fe^{III}$) within the oxide [39,40]. Decomposition then proceeds via reactions involving these two oxidation states and radical species such as OH• and HO_2•.

At high pH, this appears to have been the case for H_2O_2 decomposition on $U^{IV}_{1-2x}U^{V}_{2x}O_{2+x}$. Surfaces with this composition have been shown to support reversible redox reactions [41] and would, therefore, be expected to support H_2O_2 decomposition catalyzed by the oxidation/reduction of U^{IV}/U^{V} sites, a process which involves the incorporation and release of O^{II} interstitial species [12,32,41]. In the present study, the proximity of E_{OC} to the equilibrium potential for the anodic reaction, Fig. 1, and its closer approach to this value at higher pH when the catalytic $U^{IV}_{1-2x}U^{V}_{2x}O_{2+x}$ surface is exposed, suggests the cathodic reaction is rate determining and the pH dependence is determined, at least partially, by the increase in concentration of the HO_2^- which is the electroactive species.

4. Conclusions

The electrochemical oxidation and open circuit decomposition of H_2O_2 have been studied as a function of pH (9.5 to 12.6) and $[H_2O_2]$ (10^{-4} mol.L^{-1} to 10^{-2} mol.L^{-1}).

At pH = 9.5 the anodic oxidation is slow and appears to be blocked by the presence of an insulating U^{VI} surface layer. As the pH is increased to > 10.5 the anodic oxidation is accelerated but controlled partially by transport through a thin but chemically dissolving U^{VI} oxide/hydroxide surface layer.

At positive electrode potentials, ~ 70% of the anodic current goes to H_2O_2 oxidation and the remainder to UO_2 dissolution as UO_2^{2+} in solution of relatively high $[H_2O_2]$ (0.02 mol.L^{-1}).

At open circuit the H_2O_2 decomposition reaction rate appears to be controlled by the cathodic half reaction. At low pH ($\leq$ 10.5) it is blocked by the presence of U^{VI} surface states, but at higher pH appears to proceed rapidly on a $U^{IV}_{1-2x}U^{V}_{2x}O_{2+x}$ surface. The pH dependence of the rate suggests that HO_2^- is the electroactive form of peroxide.

The independence of E_{OC} on a range of $[H_2O_2]$ in alkaline solutions could be attributed to the decomposition of H_2O_2.

This study of the competition between the two anodic reactions (H_2O_2 oxidation and UO_2 dissolution) suggests that the H_2O_2 decomposition could be the primary pathway for H_2O_2 consumption, instead of the H_2O_2-driven UO_2 corrosion, depending on the repository conditions (e.g., surface oxidation states, H_2O_2 concentration, pH values etc.). The electrochemical studies and conclusions from this paper are consistent with the results of the recent chemical experiments [7,21,42]. Since H_2O_2, produced radiolytically, is the primary oxidant available to drive fuel dissolution inside a failed nuclear waste container, its consumption by decomposition will significantly suppress fuel corrosion rates.

Acknowledgement

This research was funded under the Industrial Research Chair agreement between the Natural Science and Engineering Research Council (NSERC, Ottawa) and the Nuclear Waste Management Organization (NWMO, Toronto). The authors thank Dr. Charles Wu for conducting the ICP test in Biotron.

References

[1] J. McMurry, D.A., Dixon, J.D., Garroni, B.M., Ikeda, S. Stroes-Gascoyne, P., Baumgartner, T.W. Melnyk, Report 06819-REP-01200-10092-R00, Ontario Power Generation, Toronto, ON, 2003.
[2] F. King, M. Kolar, Report 06819-REP-01200-10041-R00, Ontario Power Generation, Toronto, ON, 2000.
[3] F. King, M. Kolar, Mat. Res. Soc. Symp. Proc. 412 (1996) 555–562.
[4] D.W. Shoesmith, S. Sunder, J. Nucl. Mater. 190 (1992) 20–35.
[5] D.W. Shoesmith, J. Nucl. Mater. 282 (2000) 1–31.
[6] E. Ekeroth, O. Roth, M. Jonsson, J. Nucl. Mater. 355 (2006) 38–46.
[7] C.M. Lousada, M. Trummer, M. Jonsson, J. Nucl. Mater. 434 (2013) 434–439.
[8] J.S. Goldik, H.W. Nesbitt, J.J. Noël, D.W. Shoesmith, Electrochim. Acta 49 (2004) 1699–1709.
[9] J. Gimenez, E. Baraj, M.E. Torrero, I. Casas, J. de Pablo, J. Nucl. Mater. 238 (1996) 64–69.
[10] M. Trummer, S. Nilsson, M. Jonsson, J. Nucl. Mater. 378 (2008) 55–59.
[11] J.S. Goldik, J.J. Noël, D.W. Shoesmith, J. of Electroanal. Chem. 582 (2005) 241–248.
[12] B.G. Santos, J.J. Noël, D.W. Shoesmith, J. of Electroanal. Chem. 586 (2006) 1–11.
[13] J.S. Goldik, J.J. Noël, D.W. Shoesmith, J. Electrochem. Soc. 153 (2006) E151–E159.
[14] J.S. Goldik, J.J. Noël, D.W. Shoesmith, Electrochim. Acta 51 (2006) 3278–3286.
[15] D.W. Shoesmith, Report NWMO TR-2007-03, Nuclear Waste Management Organization, Toronto, ON, 2007.
[16] S. Sunder, N.H. Miller, D.W. Shoesmith, Corros. Sci. 46 (2004) 1095–1111.
[17] J. de Pablo, I. Casas, F. Clarens, F. El Aamrani, M. Rovira, Mat. Res. Soc. Symp. Proc. 663 (2001) 409–426.
[18] P. Diaz-Arocas, J. Quinones, C. Maffiotte, J. Serrano, J. Garcia, J.R. Almazan, Mater. Res. Soc. Symp. Proc. 353 (1995) 641–646.
[19] H. Christensen, R., Forsyth, R., Lundqvist, L.O., Werme, Report NS-90/85, Studsvik Energiteknik AB, Nyköping, Sweden, 1990.
[20] M. Jonsson, E. Ekeroth, O. Roth, Mater. Res. Soc. Symp. Proc. 807 (2004) 77.
[21] S. Nilsson, M. Jonsson, J. Nucl. Mater. 410 (2011) 89–93.
[22] J.C. Wren, D.W. Shoesmith, S. Sunder, J. Electrochem. Soc. 152 (2005) B470.
[23] R.I. Haines, D.R. McCracken, Proceedings of the Water Chemistry of Nuclear Reactor Systems 5 (1989) 309–310.
[24] J.A. Navarro, M.A. de la Rosa, M. Roncel, F. de la Rosa, J. Chem. Soc. Faraday Trans. 1. 80 (1984) 249–253.
[25] O. Spalek, J. Balej, I. Paseka, J. Chem. Soc. Faraday Trans. 1. 78 (1982) 2349–2359.
[26] F.R. Duke, T.W. Haas, J. Phys. Chem. 65 (1961) 304–306.
[27] Y. Zhang, G.S. Wilson, J. Electroanal. Chem. 345 (1993) 253–271.
[28] J.O.M. Bockris, L.F. Oldfield, Trans. Faraday Soc. 51 (1955) 249–259.
[29] P.G. Lucuta, R.A. Verrall, H.-J. Matzke, B.J.F. Palmer, J. Nucl. Mater. 178 (1991) 48–60.
[30] D.W. Shoesmith, W.H. Hocking, S. Sunder, J.S. Betteridge, N.H. Miller, J. Alloys Compd. 213/214 (1994) 551.
[31] I. Grenthe, J. Fuger, R.J. Konings, R.J. Lemire, A.B. Muller, C. Nguyen-Trung, H. Wanner, Chemical Thermodynamics of Uranium, North Holland, Armsterdam, 1992.
[32] B.G. Santos, H.W. Nesbitt, J.J. Noël, D.W. Shoesmith, Electrochim. Acta 49 (2004) 1863–1873.
[33] A.J. Bard, L.R. Flaukner, Electrochemical Methods: Fundamentals and Applications, 2nd ed., John Wiley & Sons, New York, NY, 2001.
[34] C.A. Bunton, H.J. Foroudian, Langmuir 9 (1993) 2832–2835.
[35] A. Hickling, W.H. Wilson, J. Electrochem. Soc. 98 (1951) 425–433.
[36] A. Hiroki, J.A. LaVerne, J. Phys. Chem. B 109 (2005) 3364–3370.
[37] C.M. Lousada, A.J. Johansson, T. Brinck, M. Jonsson, J. Phys. Chem. C 116 (2012) 9533–9543.
[38] C.M. Lousada, M. Jonsson, J. Phys. Chem. C 114 (2010) 11202–11208.
[39] S.S. Lin, M.D. Gurol, Environ. Sci. Technol. 32 (1998) 1417–1423.
[40] D. Fu, X. Zhang, P.G. Keech, D.W. Shoesmith, J.C. Wren, Electrochim. Acta 55 (2010) 3787–3796.
[41] H. He, Z. Ding, D.W. Shoesmith, Electrochem. Comm. 11 (2009) 1724–1727.
[42] R. Pehrman, M. Trummer, C.M. Lousada, M. Jonsson, J. Nucl. Mater. 430 (2012) 6–11.